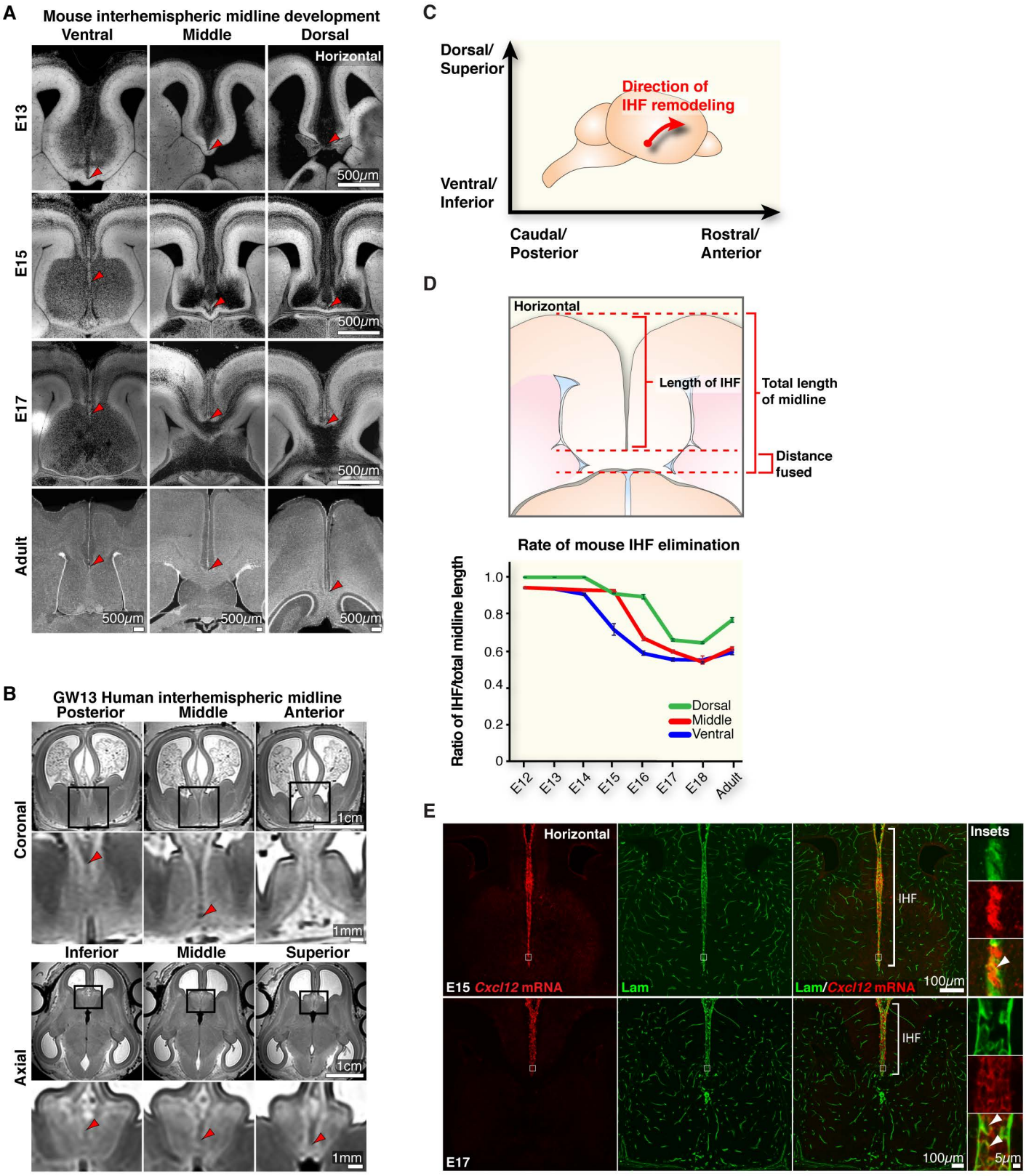

Figure S1 (related to Figure 2)

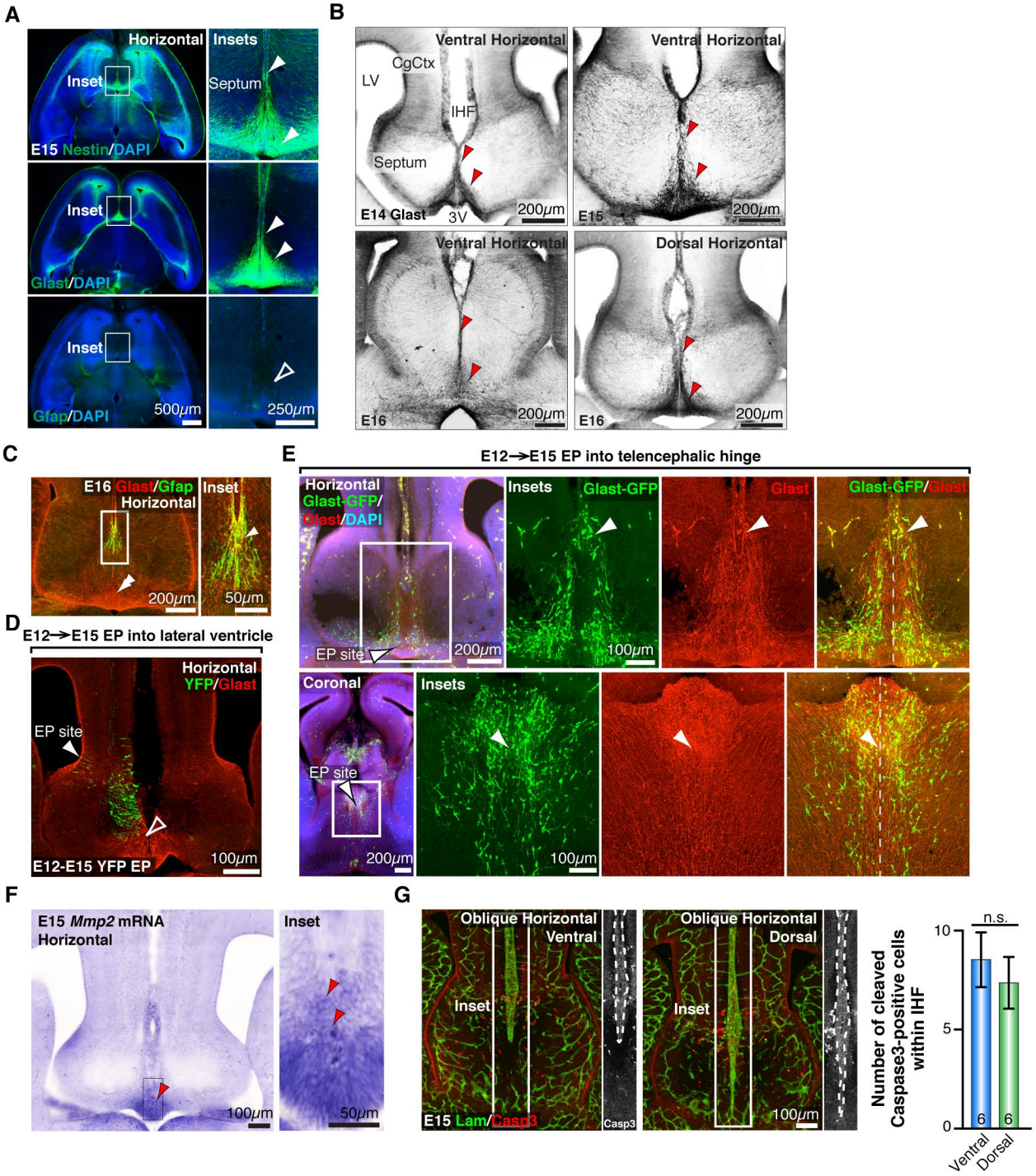

Figure S2 (related to Figure 3)

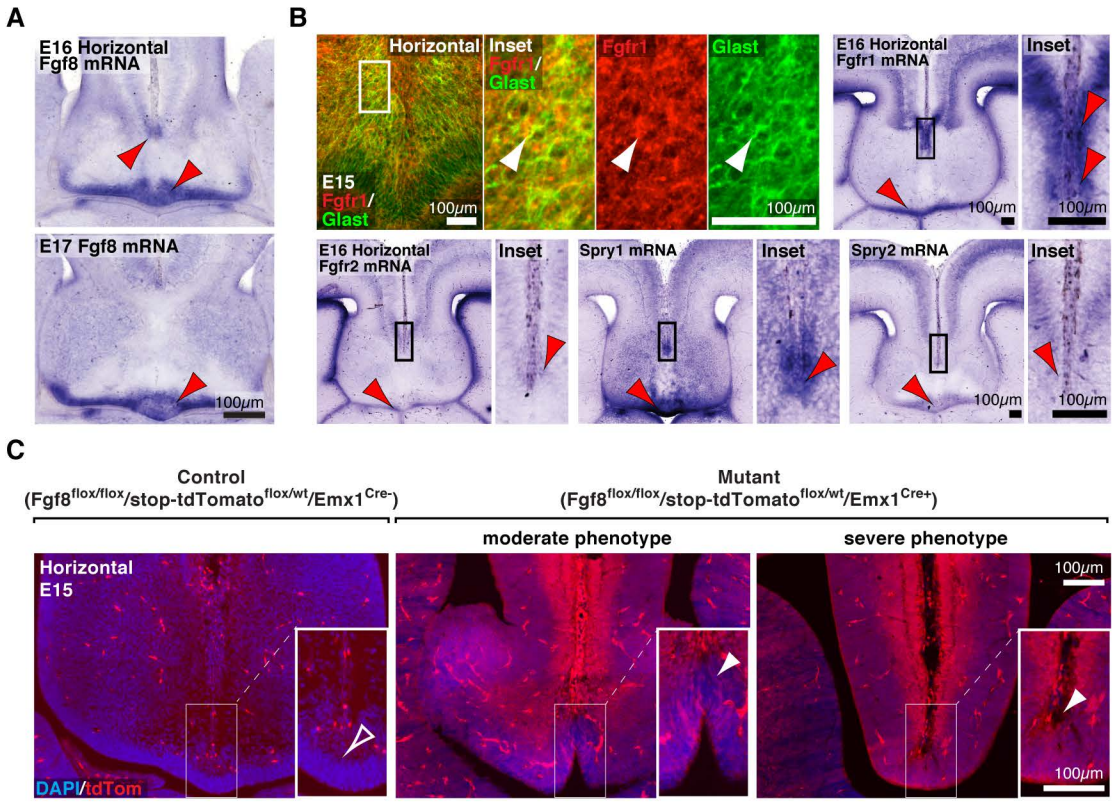

Figure S3 (related to Figure 4)

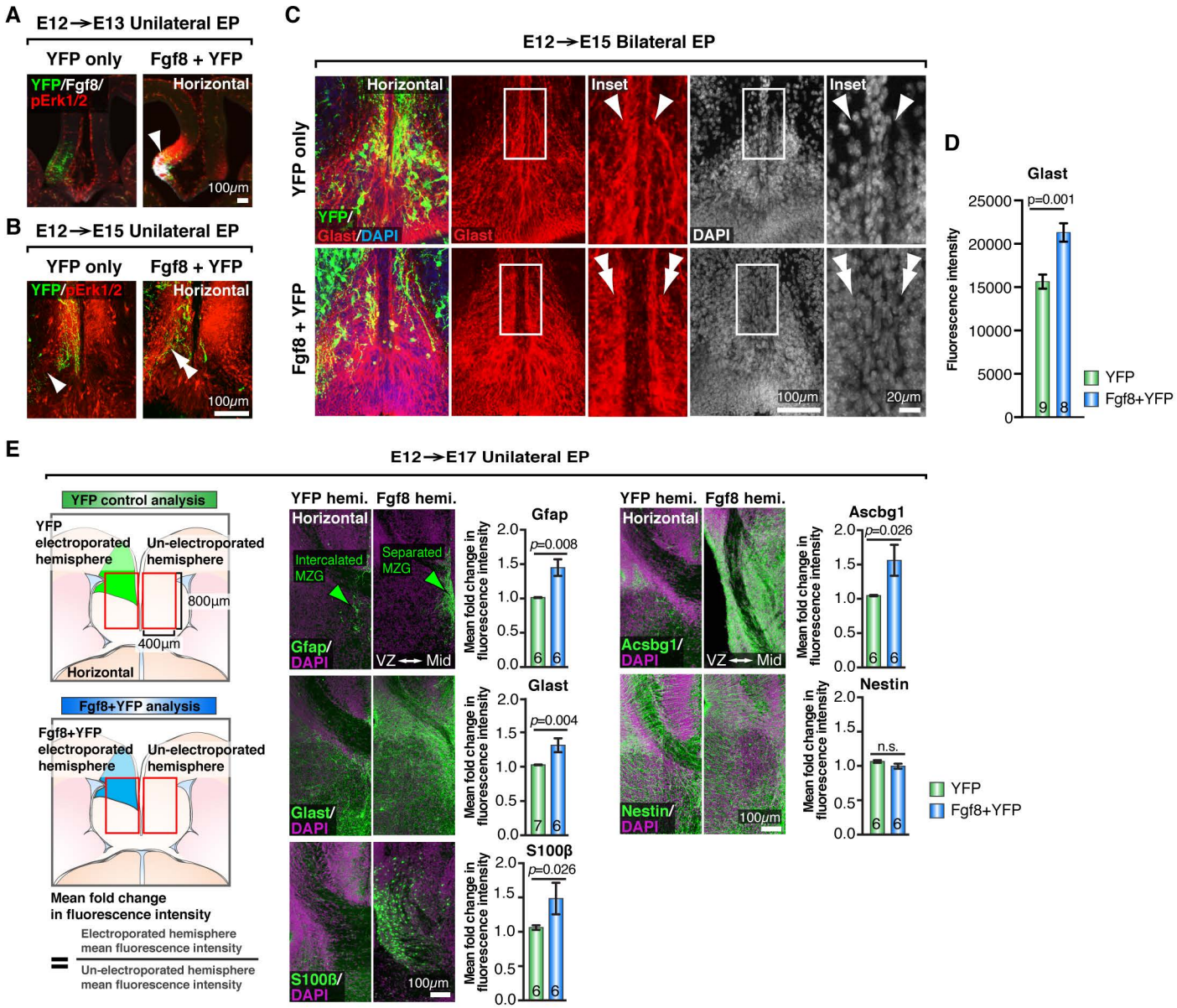

Figure S4 (related to Figure 5)

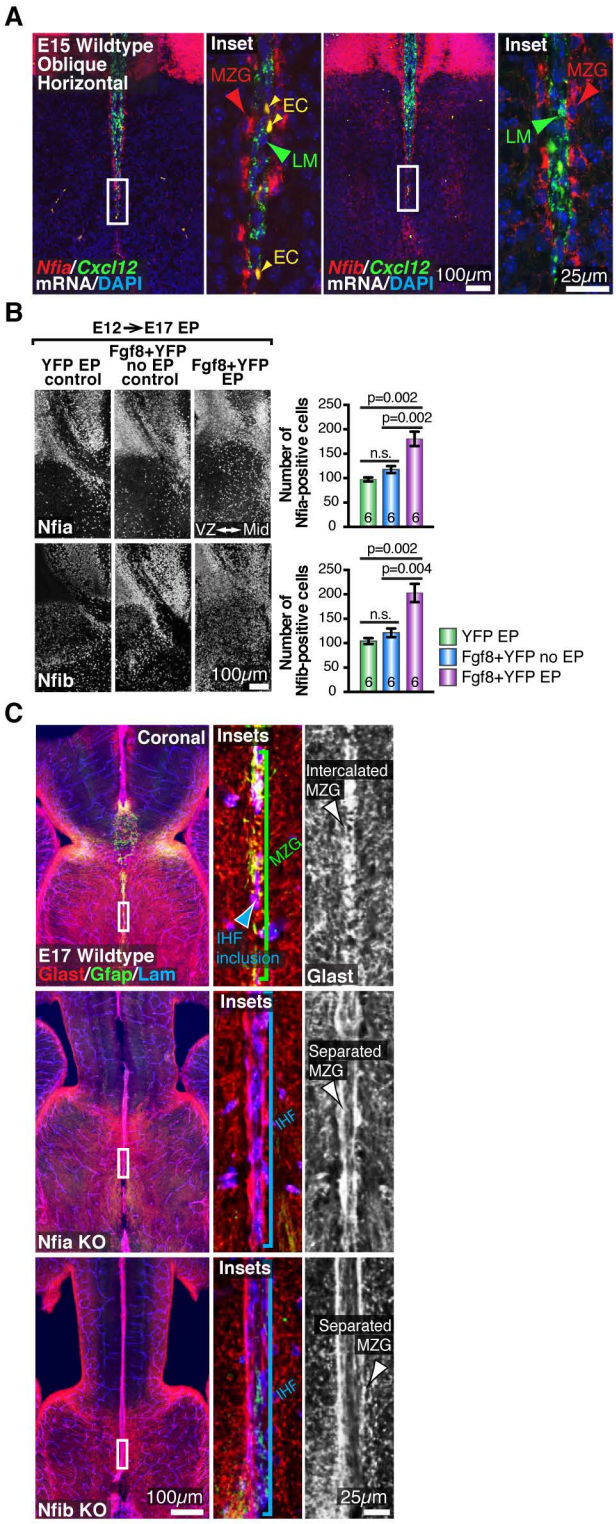

Figure S5 (related to Figure 6)

Supplemental Figure Legends

Figure S1 (related to Figure 2): Analysis of IHF remodeling in the developing mouse and human brain.
(A) Representative horizontal images of the ventral, middle and dorsal regions of the mouse telencephalic midline at different developmental stages, stained with the nuclear marker DAPI. Red arrowheads indicate the base of the IHF. (B) Serial coronal and axial T1-weighted structural MRI images of the human telencephalic midline at gestational week (GW)13, during remodeling of the IHF. Red arrowheads indicate the base of the IHF. (C) Schema in sagittal orientation indicating the oblique trajectory of IHF remodeling in mice and humans. (D) Schema indicating measurements used to determine the rate of IHF elimination in mice, quantified below. Data points are representative of the ratio of IHF length to total midline length ± SEM per stage. For each mouse embryonic stage, n ≥ 6 brains were measured from matched ventral, middle and dorsal regions of the telencephalon. (E) Fluorescent in situ hybridization for *Cxcl12* mRNA (red) and fluorescent immunohistochemistry for pan-Laminin (green) at E15 and E17. Note colocalization of *Cxcl12* and Laminin within the cell bodies of leptomeningeal fibroblasts (arrowheads). Brackets denote the extent of the IHF at each developmental stage.

Figure S2 (related to Figure 3): Characterization of MZG development and leptomeningeal elimination.
(A) Fluorescence immunohistochemistry for Nestin, Glast and Gfap glial protein expression during the initiation of IHF remodeling at E15; closed arrowheads indicate the high expression of Nestin and Glast and open arrowhead indicates the absence of Gfap expression. (B) Developmental time course of Glast expression throughout the peak period of IHF remodeling, red arrowheads indicate expression of Glast in radial MZG progenitors. (C) Fluorescence immunohistochemistry showing colocalization of Glast and Gfap in intercalated multipolar MZG cells at E16. In utero electroporation (EP) of (D) the lateral ventricular zone and (E), the telencephalic hinge, with either YFP or *piggyBac* Glast transposase/GFP reporter plasmids followed by GFP/Glast immunohistochemistry; note absence of colocalization in D (open arrowhead) and colocalization in E (closed arrowheads). (F) In situ hybridization for *Mmp2* mRNA, where red arrowheads indicate the spatial overlap of *Mmp2* expression with MZG cells. (G) Fluorescence immunohistochemistry for apoptotic cleaved-Caspase3 and Laminin within the IHF before (dorsal), and after (ventral), remodeling at E15, with quantification of the mean number of cleaved-Caspase3-positive cells within the IHF. Data are represented as means ± SEM (n-values within bars). Significant differences were determined with a non-parametric Mann-Whitney test. CgCtx = cingulate cortex, LV = lateral ventricle, 3V = third ventricle.

Figure S3 (related to Figures 4): Fgf8 signaling is required for MZG development and interhemispheric remodeling in mice.
(A) In situ hybridization for *Fgf8* mRNA and (B) fluorescence immunohistochemistry for Fgfr1 protein and the MZG marker Glast, as well as in situ hybridization for *Fgfr1*, *Fgfr2*, *Spry1* and *Spry2* mRNA. Arrowheads indicate the colocalization of Fgfr1 protein with Glast-positive radial MZG undergoing somal translocation (white arrowheads), as well as the spatial overlap of mRNA signals with the radial MZG progenitors within the telencephalic hinge and those undergoing somal translocation to the base of the IHF (red arrowheads). (C) Expression of tdTomato resulting from Cre-mediated recombination in E15 conditional Fgf8*flox*/flox-stop-flox-tdTomato/Emx1*Cre*-positive mutants and Cre-negative littermate controls. Closed arrowheads denote successful Cre-mediated recombination in the radial MZG progenitor niche.

Figure S4 (related to Figure 5): Fgf8 signaling promotes astroglial maturation of the MZG in mice.
(A) Unilateral E12→E13 in utero electroporation (EP) of YFP alone or coelectroporation of Fgf8 + YFP plasmids followed by fluorescence immunohistochemistry for YFP, Fgf8 and phospho-Erk1/2 (pErk1/2). Arrowhead indicates ectopic upregulation of Fgf8 and pErk1/2 proteins following Fgf8 EP. (B) Unilateral E12→E15 EP of YFP alone or coelectroporation of Fgf8 + YFP plasmids followed by fluorescence immunohistochemistry for YFP and phospho-Erk1/2. Single arrowhead indicates normal p-Erk1/2 in radial MZG progenitors undergoing somal translocation to the IHF and double arrowhead indicates the increased number of p-Erk1/2-positive radial MZG following Fgf8 EP. (C) Bilateral E12→E15 EP of YFP alone or coelectroporation of Fgf8 + YFP plasmids followed by fluorescence immunohistochemistry for YFP (green), Glast (red), and DAPI nuclear staining (white). Note excess Glast-positive cell bodies along the pial surface of the Fgf8-electroporated hemispheres (double arrowheads) compared to the YFP-only electroporated hemispheres (single arrowheads). Quantification of the mean Glast fluorescence intensity in YFP versus Fgf8+YFP electroporated hemispheres is shown in (D). (E) Unilateral E12→E17 EP of Fgf8 + YFP plasmids followed by fluorescence immunohistochemistry for the mature astroglial proteins Gfap, Glast, S100ß, and

Acsbg1, and the radial glial protein Nestin (in green). Expression of each marker was quantified in both YFP control and Fgf8 + YFP brains as the mean fold change in fluorescence intensity between the electroporated and unelectroporated hemispheres. Note significant upregulation of astroglial proteins following Fgf8 EP. Data are represented as means ± SEM (n-values within bars). Significant differences were determined with a non-parametric Mann-Whitney test. Mid = midline, VZ = ventricular zone.

Figure S5 (related to Figure 6): Nfia and Nfib are downstream transcriptional effectors of Fgf8 signaling required for IHF remodeling and corpus callosum formation.
(A) Double fluorescent in situ hybridization for *Nfia* or *Nfib* mRNA (red) with *Cxcl12* mRNA (green) at E15. Note absence of fluorophore colocalization except in anuclear erythrocytes (EC; yellow arrowheads). Red and green arrowheads denote the MZG and leptomeningeal fibroblasts (LM), respectively. (B) Unilateral E12→E17 EP of Fgf8 + YFP plasmids followed by fluorescence immunohistochemistry for Nfia and Nfib. The mean number of Nfia- or Nfib-positive cells along the midline is quantified on the right. (C) Fluorescence immunohistochemistry for Glast, Gfap and Laminin in Nfia and Nfib knockout (KO) embryos and wildtype littermates at E17 in coronal view. Brackets indicate the extent of intercalated MZG versus IHF in each condition, and arrowheads indicate the morphology of the MZG. Data are represented as means ± SEM (n-values within bars). Significant differences were determined with a non-parametric Mann-Whitney test. Mid = midline, VZ = ventricular zone.

Supplemental Table 1 (related to Figure 7): Interhemispheric fissure phenotype associated with human callosal agenesis[a].

	Number of cases	Percentage of total (56 cases)
Complete callosal agenesis - with complete retention of the interhemispheric fissure	38	67.8%
Anterior callosal agenesis - with anterior retention of the interhemispheric fissure	4	7.1%
Callosal agenesis - could not assess extent of the interhemispheric fissure[b]	14	25.0%

[a]Table showing the total number of isolated callosal agenesis cases analyzed (56 cases), separated into interhemispheric fissure phenotypes.

[b]Note that the MRI studies from 14 individuals could not be assessed for interhemispheric fissure phenotype due to inadequate clinical scan quality.

Supplemental Experimental Procedures

Plasmid expression constructs used for in utero electroporation

Plasmid expression constructs used were pCAG-YFP (kind gift from Tetsuichiro Saito, Chiba University, Japan), pCAG-DsRed2 (Addgene, plasmid 15777), pEFX-Fgf8 (kind gift from Tomomi Shimogori, RIKEN Brain Science Institute, Japan), pGlast-PBase and pPBCAG-eGFP (kind gift from Joseph LoTurco, University of Connecticut, USA), and pCAG-myr-tdTomato-2A-H2B-GFP (kind gift from Arnold Kriegstein, UCSF, USA).

Antibodies and reagents used for immunohistochemistry

Primary antibodies used for immunohistochemistry were as follows: rabbit anti-DsRed (1:1000; 632496, Clontech), mouse anti-Gap43 (1:500; AB1987, Millipore), mouse anti-Gfap (1:500; MAB3402, Millipore), rabbit anti-Gfap (1:500; Z0334, Dako), chicken anti-Gfp (1:1000; ab13970, Abcam), rabbit anti-Gfp (1:1000; A6455, Invitrogen), mouse anti-Glast (or Eaat1; 1:500; ab49643, Abcam), rabbit anti-Glast (or Eaat1; 1:250; ab416, Abcam), mouse anti-Fgf8 (1:250; MAB323, R&D Systems), mouse anti-Fgfr1 (1:250; ab823, Abcam), chicken anti-Laminin (1:500; LS-C96142, LSBio), rabbit anti-Laminin (1:500; L9393, Sigma), mouse anti-Nestin (1:250; rat-401, Developmental Studies Hybridoma Bank), rabbit anti-Nfia (1:500; ARP32714, Aviva Systems Biology; and 39329, Active Motif), rabbit anti-Nfib (1:500; HPA003956, Sigma), rabbit anti-neuronal-specific-ßIII-tubulin (1:500; ab18207, Abcam) and rabbit anti-phospho p44/42 Mapk (or Erk1/2; 1:250; 9101, Cell Signaling). Alexa Fluor IgG (Invitrogen), horseradish peroxidase-conjugated (Millipore) or biotinylated-conjugated (Jackson Laboratories) secondary antibodies, used in conjunction with Vectastain Elite ABC (Vector Laboratories), TSA Plus Fluorescence Systems (Perkin-Elmer) or Alexa Fluor 647-conjugated Streptavidin (Invitrogen) amplification, were all used according to the manufacturer's instructions. Sections were counterstained to label cell nuclei using haematoxylin (Sigma) or 4',6-diamidino-2-phenylindole, dihydrochloride (DAPI, Invitrogen) and coverslipped using DPX (Ajax Finechem) or ProLong Gold anti-fade reagent (Invitrogen) mounting media.

In situ hybridization

In situ hybridization was performed as previously described (Moldrich et al., 2010). *Fgfr1* and *Fgfr2* cDNA plasmids (Tole et al., 2006) were kind gifts from Shubha Tole, Tata Institute of Fundamental Research. *Fgf8*, *Sprouty1*, and *Sprouty2* cDNA plasmids (Crossley and Martin, 1995; Minowada et al., 1999), were kind gifts from Gail Martin, University of San Francisco. The *Cxcl12*, *Mmp2*, *Nfia* and *Nfib* cDNA plasmids were generated in-house with primers corresponding to those used in the Allen Developing Mouse Brain Atlas (Website: © 2015 Allen Institute for Brain Science. Allen Developing Mouse Brain Atlas [Internet]. Available from: http://developingmouse.brain-map.org).

Image acquisition

Brightfield and wide-field fluorescence imaging were performed with a Zeiss upright Axio-Imager Z1 microscope fitted with Axio- Cam HRc and HRm cameras and Apotome. Images were acquired with AxioVision software (Carl Zeiss). Confocal images were acquired as either single 0.6 μm optical sections or multiple image projections of ~10 μm thick z-stacks using an LSM 710 NLO confocal microscope and Zen 2012 software (Carl Zeiss) or a Zeiss inverted Axio-Observer fitted with a W1 Yokogawa spinning disk module and Hamamatsu Flash4.0 sCMOS camera and Slidebook 5.5 software. Images were pseudocolored to permit overlay, and then were cropped, sized, and contrast-brightness enhanced for presentation with Photoshop software (Adobe).

Fluorescence intensity quantification following Fgf8 overexpression

For fluorescence intensity analyses, a region of interest (ROI) within each brain hemisphere was cropped from fluorescence images using Photoshop CS5.1 (Adobe) and imported into ImageJ. To minimize inter-brain variability, anatomical landmarks consistent across all experimental conditions were used to position ROIs. For Fgf8

overexpression analyses, ROIs were positioned adjacent to the midline and aligned to the rostral-most extent of the lateral ventricles. The ROI dimensions were 30 μm by 150 μm for the E12-E15 Fgf8/YFP electroporations, and 410 μm by 800 μm for the E12-E17 and E14-E17 Fgf8/YFP electroporations. The fluorescence intensity was then plotted and averaged over the width of the ROI and expressed either as the number of gray values or the fold change ratio to the un-electroporated hemisphere following unilateral electroporations.

Cell counts

For cell birthdating studies, 5-ethynyl-2´-deoxyuridine (EdU; 5 mg per kg body weight, Invitrogen) was injected intraperitoneally into awake pregnant dams. Following sacrifice, tissue was processed for Glast immunohistochemistry and EdU labeling using the Click-iT EdU Alexa Fluor 488 Imaging Kit (Invitrogen). The number of Glast/EdU double-positive MZG cells born at each age were counted by segmenting out the Glast-positive telencephalic hinge region and masking the IHF where present, in ImageJ. The number of EdU-positive cells present within this ROI were then counted double-blind using the ImageJ Cell counter plugin. Average ROI surface areas were 0.075 ± 0.012 mm^2 (E13); 0.113 ± 0.017 mm^2 (E14); 0.195 ± 0.037 mm^2 (E15); and 0.267 ± 0.069 mm^2 (E16) from 6-7 brains per embryonic age. Counts of Nfia and Nfib-positive cells in Fgf8 overexpression experiments were made as above, from a 30 μm by 800 μm ROI aligned to the interhemispheric midline. Counts of translocated Glast-positive MZG cells in Fgf8 cKO mutants and littermate controls were performed as above with an average ROI surface area of 4488μm^2 ± 3386 μm^2.

Ex-vivo magnetic resonance imaging

T1-weighted structural magnetic resonance imaging (MRI) of a fixed whole GW 13 human brain was performed at The University of Queensland by incubating for 4 days in PBS containing 0.5 mM Magnevist®, followed by image acquisition using a 16.4 T scanner equipped with Micro2.5 gradient (Bruker Biospin, Karlsruhe, Germany) and a 25 mm microimaging SAW volume coil (M2M Imaging, Australia). 3D T1-weighted gradient echo was acquired at 22ºC, using FLASH (Fast Low Angle Shot, Paravision 5.1) with the following parameters: flip angle 30 degrees, TR/TE=50/8 ms, NEX=8 and partial Fourier acceleration factor of 1.34 in the phase dimensions, 0.1 mm isotropic resolution.

Scanning electron microscopy

Whole embryonic mouse heads or dissected brain samples were post-fixed in osmium tetroxide and dehydrated in a graded series of ethanol before being dried in a critical point dryer (Austosamdri-815, Tousimis). Samples were then mounted on aluminum stubs and gold coated in a sputter coater (SPI Supplies). Samples were imaged in a JCM-5000 Neoscope (JEOL) at an accelerating voltage of 10kV.

Cell culture and Gfap *luciferase reporter assay*

Plates (96-wells) were seeded with 3000 U251 glioblastoma cells per well and maintained in DMEM (Life Technologies), supplemented with 10% fetal bovine serum (SAFC Biosciences). After 24 hours, a mouse *Gfap* promoter luciferase plasmid (Zhou et al., 2004) was co-transfected with either pCAG-*Nfia*-IRES-GFP, pCAG-*Nfib*-IRES-GFP (Piper et al., 2010) or the control pCAG-IRES-GFP plasmid (Addgene, plasmid 11159) into these cells. The *Renilla* luciferase vector (pRL-SV40, Promega) was co-transfected as an internal control in all experiments. Twenty-four hours after transfection, the cell culture medium was refreshed with 5 or 20μM Mek inhibitor U0126 (Cell Signaling) or vehicle control (DMSO). Cells were then lyzed 24 hours later and luciferase activity was measured using the Dual-Luciferase Reporter Assay system (Promega) on a POLARstar OPTIMA plate reader (BMG Labtech). All experimental conditions were conducted in triplicate, in at least 2 independent experiments, and analyzed with a Student's *t*-test, $p \leq 0.05$ was considered significantly different.

Supplemental References

Crossley, P.H., and Martin, G.R. (1995). The mouse Fgf8 gene encodes a family of polypeptides and is expressed in regions that direct outgrowth and patterning in the developing embryo. Development *121*, 439-451.

Minowada, G., Jarvis, L.A., Chi, C.L., Neubuser, A., Sun, X., Hacohen, N., Krasnow, M.A., and Martin, G.R. (1999). Vertebrate Sprouty genes are induced by FGF signaling and can cause chondrodysplasia when overexpressed. Development *126*, 4465-4475.

Moldrich, R.X., Gobius, I., Pollak, T., Zhang, J., Ren, T., Brown, L., Mori, S., De Juan Romero, C., Britanova, O., Tarabykin, V., *et al*. (2010). Molecular regulation of the developing commissural plate. J Comp Neurol *518*, 3645-3661.

Piper, M., Barry, G., Hawkins, J., Mason, S., Lindwall, C., Little, E., Sarkar, A., Smith, A.G., Moldrich, R.X., Boyle, G.M., *et al*. (2010). NFIA controls telencephalic progenitor cell differentiation through repression of the Notch effector Hes1. J Neurosci *30*, 9127-9139.

Tole, S., Gutin, G., Bhatnagar, L., Remedios, R., and Hebert, J.M. (2006). Development of midline cell types and commissural axon tracts requires Fgfr1 in the cerebrum. Dev Biol *289*, 141-151.

Zhou, B.Y., Liu, Y., Kim, B., Xiao, Y., and He, J.J. (2004). Astrocyte activation and dysfunction and neuron death by HIV-1 Tat expression in astrocytes. Mol Cell Neurosci *27*, 296-305.